

# Generation of Impossible Cross-Peaks Between Bulk Water and Biomolecules in Solution NMR

Warren S. Warren, Wolfgang Richter, Amy Hamilton Andreotti, Bennett T. Farmer II

Intermolecular multiple-quantum coherences between bulk water and a glycoprotein fragment at modest concentration (20 mM) have been experimentally produced and detected, although such coherences are inconceivable in the normal theoretical framework of nuclear magnetic resonance. A density matrix treatment explains these results by including the long-range dipolar interaction between spins and by discarding the high-temperature approximation. These results imply that peak intensities (critical for structural determinations) can be distorted in many gradient experiments, and show that magic-angle gradients provide substantial improvements with reduced gradient strengths. They also suggest methods for contrast enhancement in magnetic resonance imaging.

Nuclear magnetic resonance (NMR) is an extremely versatile form of spectroscopy, in part because commercially available spectrometers can generate exceedingly complex pulse sequences. More importantly, however, quite sophisticated theoretical tools have been developed over the last half century. It is really the ability to predict the effects of dozens or hundreds of radio-frequency (RF) and field gradient pulses on complex samples (such as proteins) which has made NMR so valuable for structural studies in solution (1).

It was thus disconcerting to see that NMR spectra of even a sample as simple as pure water can differ greatly from these predictions (2–4). If the water is placed off resonance by an amount  $\Delta\omega$ , the normal theory of NMR or magnetic resonance imaging (MRI) predicts that the only evolution frequencies will be  $\Delta\omega$  (from the transverse magnetization  $M_x$  or  $M_y$ , precessing in the static magnetic field) or zero (from the longitudinal magnetization  $M_z$ ) (5). Instead, two-dimensional (2D) NMR spectra can show strong and unexpected peaks at frequencies  $n\Delta\omega$  in the indirectly detected dimension (2–4). Such frequencies are generally associated with multiple-quantum coherences (superpositions of two eigenstates of the spin system, separated in energy by more than one spin flip). In fact, one of the most powerful techniques for isolating multiple-quantum coherences [a coherence transfer echo (6), which uses two gradient pulses in a 1:n length ratio to isolate  $n$ -quantum coherences] produces intermolecular cross-peaks (4). These peaks survive all of the experimental tests that would distinguish multiple-quantum coherences from spectrometer artifacts.

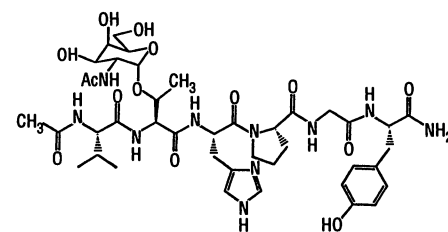
We show here that extremely simple pulse sequences generate intense intermolecular cross-peaks between bulk water and a fragment of the glycoprotein fibronectin at modest concentration, even though such coherences are not predicted in normal NMR theory. We also present a conventional density matrix calculation (with two critical additions) that predicts the observed strong intermolecular multiple-quantum cross-peaks when at least one species is concentrated. First, we discard the normal high-temperature approximation [ $\rho_{\text{eq}} \approx 1 - (\gamma B_0 \beta) I_z$ ] where  $\rho_{\text{eq}}$  is the equilibrium density matrix,  $\gamma$  is the gyromagnetic ratio,  $B_0$  is the applied static magnetic field,  $\beta$  is the reciprocal of the product of Boltzmann's constant and temperature (thermal energy), and  $I_z$  is the magnetization in the  $z$  direction]; even the first neglected term [ $(\gamma B_0 \beta) I_z$ ]<sup>2</sup>/2 generates zero-quantum and two-quantum coherences after a single pulse. In addition, we explicitly retain the dipole-dipole interaction between spins separated by distances greater than diffusion lengths on an NMR time scale ( $\sim 10 \mu\text{m}$ ). At first glance, both of these modifications seem irrelevant; the additional factor of  $(\gamma B_0 \beta) \approx 10^{-4}$  in front of the two-quantum term would seem to justify truncation, and the dipole field generated by a single proton is less than  $10^{-16}$  T at  $10 \mu\text{m}$ . However, there are  $\sim 10^{45}$  different pairs of spins in a typical 1-ml sample. We will show that the combination of these two effects can transfer intermolecular multiple-quantum coherences into observable magnetization and produce signals comparable in size to the magnetization generated by a single pulse. We also discuss the implications of these results for NMR structural determinations and for MRI.

We will restrict our attention here to one pulse sequence (Fig. 1) that has two strong RF pulses and two  $z$ -gradient pulses of unequal lengths (4). This can be viewed as the simplest 2D experiment [a correlated spec-

troscopy (COSY) sequence (1)] modified to select two-quantum coherences during time  $t_1$ . We call this a CRAZED sequence (COSY revamped with asymmetric  $z$ -gradient echo detection), in part because, to an experienced NMR spectroscopist, it looks crazed; in the standard density matrix formalism (1), a CRAZED sequence must give blank spectra because COSY sequences do not produce two-quantum coherences during  $t_1$ .

Nonetheless, this sequence gives large signals in concentrated solutions. We have previously published (4) a variety of CRAZED experiments on concentrated solutions of molecules with only equivalent spins in each molecule (such as water, benzene, chloroform, or acetone). A mixed sample (such as benzene and chloroform) gives the normal two-line spectrum in the directly detected ( $F_2$ ) dimension, but neither of the normal transition frequencies appears in the indirectly detected ( $F_1$ ) dimension (4). Instead, we see strong peaks at twice the benzene frequency, twice the chloroform frequency, and the sum of the benzene and chloroform frequencies—as expected for the three conceivable (but normally unobservable) two-quantum coherences involving two spins of different molecules. All of the observed phase shift, diffusion, and gradient echo properties are those expected for multiple-quantum coherences (7).

In fact, only one of the species in solution needs to be concentrated to see these effects, which implies that they can be important for biomolecules in water. Figure 2 shows the 600-MHz CRAZED spectrum of a 20 mM solution of a fibronectin fragment in water. This glycosylated hexapeptide represents the minimal structural requirement for monoclonal antibody (FDC-6) recognition of fibronectin in fetal and malignant cells (8). In this spectrum, the water peak



is at frequency  $\nu_{\text{H}_2\text{O}} = \Delta\omega/2\pi = 530 \text{ Hz}$  below resonance ( $-0.88 \text{ ppm}$ ). Again, the spectrum should be blank. Instead, an intense water peak plus glycopeptide resonances are seen in the directly detected ( $F_2$ ) dimension (no solvent suppression was attempted here). However, virtually no diagonal ( $F_1 = F_2$  or  $F_1 = -F_2$ ) peaks survive anywhere in the spectrum; in fact, no peaks in  $F_1$  appear at the frequencies of the water or glycopeptide resonances. A double-quantum water resonance does survive ( $F_1 =$

W. S. Warren, W. Richter, A. Hamilton Andreotti, Department of Chemistry, Princeton University, Princeton, NJ 08544-1009.

B. T. Farmer II, Bristol-Myers-Squibb Pharmaceutical Research Institute, Bristol-Myers-Squibb, P.O. Box 4000, Princeton, NJ 08543-4000.

$-2\nu_{\text{H}_2\text{O}}$  and  $F_2 = \nu_{\text{H}_2\text{O}}$ , as expected from earlier work. In addition, most of the glycopeptide resonances show peaks at  $F_1 = -(F_2 - 530 \text{ Hz})$ , the predicted frequency of a heteromolecular two-quantum coherence involving water and glycopeptide. Finally, the normal COSY spectrum has cross-peaks induced by  $J$  couplings; similar peaks, again shifted by the water frequency, are seen in our spectra. The gradient pulse length  $T$  was varied from 1 to 10 ms with generally similar results.

The CRAZED sequence is presented here as the simplest example of an extremely general phenomenon. We find extra peaks after many different pulse sequences that use unequal-length gradient pulses (a common technique for solvent suppression). Placing the water peak exactly on resonance, as is commonly done in biological applications, makes them overlap with other, expected cross-peaks and diagonal peaks. However, in this case they still distort intensities. Peak intensities [particularly from nuclear Overhauser effect (NOE) experiments] play a crucial role in NMR structural determination, so such distortions can lead to incorrect data interpretation.

For simplicity, we will focus first on using the density matrix formalism to describe the CRAZED spectrum of the solvent peak alone. Any system with only equivalent protons (such as water or benzene) is identical because the  $J$  coupling can be ignored. The full Hamiltonian between RF pulses (in the usual "rotating frame") is:

$$\mathcal{H} = \hbar \left[ (\Delta\omega + \gamma Gs) \sum_{i=1}^N I_{zi} + \sum_{i=1}^N \sum_{j=1}^N D_{ij} (3I_{zi}I_{zj} - \mathbf{I}_i \cdot \mathbf{I}_j) \right] \quad (1)$$

$$D_{ij} = (\mu_0/4\pi) [3\cos^2\theta_{ij} - 1] |r_{ij}|^{-3} (\hbar\gamma^2)/4 \quad (2)$$

for  $r_{ij} > r_{\text{cutoff}}$ ; otherwise  $D_{ij} = 0$ . Here  $\hbar$  is Planck's constant divided by  $2\pi$ ,  $|r_{ij}|$  is the

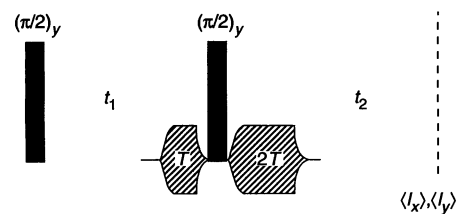


**Fig. 1.** A CRAZED pulse sequence. This sequence can be viewed as a two-pulse COSY sequence modified to include a pair of gradient pulses as a coherence transfer echo. The observable magnetization ( $I_x$  or  $I_y$ ) comes entirely from one-quantum operators. The 1:2 length ratio of the two gradient pulses guarantees that only coherences that evolved as two-quantum operators during  $t_1$  will be refocused.

separation between spins  $i$  and  $j$ , and  $\theta_{ij}$  is the angle the interspin vector makes with the applied static field  $B_0\hat{z}$ .  $N$  is the number of spins in the sample,  $G$  is the strength of a pulsed gradient of the  $z$  magnetic field which is directed along some arbitrary direction  $\hat{s}$ , and  $s = \mathbf{r} \cdot \hat{s}$  gives the distance from the origin along the  $s$  direction; this term is only present when the gradient pulses are on. For the experiment in Fig. 2,  $\hat{s} = \hat{z}$ .

The  $D_{ij}$  terms in Eqs. 1 and 2, which reflect the interaction between magnetic dipoles, are orientation dependent and thus are usually assumed to be averaged away by diffusion (in our notation,  $r_{\text{cutoff}} \rightarrow \infty$ ). However, this averaging cannot occur for spins separated by more than the distance molecules can travel by diffusion on an NMR time scale ( $\sim 10 \mu\text{m}$  for small molecules). The parameter  $r_{\text{cutoff}}$  clearly depends on the diffusion constant and the separation between pulses, but none of our final results will depend on the exact value.

The retained individual couplings are very small because the dipole-dipole interaction falls off as  $|r_{ij}|^{-3}$ . However, the total number of spins at a given distance  $|r|$  is proportional to  $|r|^2$ ; so if it were not for the angular averaging, the total interaction energy between one spin and all of the spins at a fixed distance  $|r|$  would only fall off as  $1/r$ . For an infinitely large sample, this sum diverges—the contribution made by spins between, for example, 1 and 3 mm from any given spin is just as large as the contribution made by spins between 1 and 3  $\mu\text{m}$  or 1 and 3 nm. Fortunately, the angular dependence makes this sum vanish for an isotropic distribution ( $\langle 3\cos^2\theta - 1 \rangle = 0$ ). If the spatial distribution is

made nonuniform (by gradient pulses), this angular cancellation does not hold and dipolar effects can reappear.

One way to handle this effect is to modify the Bloch equations by a mean-field approximation [the "dipolar demagnetizing field"  $B_d(r)$  (9–14)] which replaces individual spins with the local average magnetization. The magnitude (in angular frequency units) of this field is  $\sim \gamma\mu_0 M_0$ ; in our previous paper using this treatment (4) we defined  $(\gamma\mu_0 M_0)^{-1}$  as the "dipolar demagnetizing time"  $\tau_d$ ; for water at room temperature in a 600-MHz spectrometer,  $\tau_d \approx 70$  ms. However, the modified Bloch equation treatment generates equations of motion that violate Schrödinger's equation—the propagator depends explicitly on the initial state of the system (4). It also does not appear to agree with experimental results from more complex sequences (4) (more than two pulses).

A density matrix treatment is far more general. The equilibrium density matrix is (where  $I_f$  indicates lab frame):

$$\rho_{\text{eq}} = \exp(-\beta\mathcal{H}_f) / \text{Tr}[\exp(-\beta\mathcal{H}_f)] \quad (3)$$

The energy separation between spin states ( $\hbar\omega_0$ ) is small compared to the thermal energy  $\beta^{-1}$  at room temperature; for protons in a 600-MHz spectrometer,  $\beta\hbar\omega_0 \approx 10^{-4}$ . This leads to the conventional (high-temperature) power series approximation (1):

$$\rho_{\text{eq}} \approx 2^{-N} \left( \left\{ 1 - \beta\hbar\omega_0 \sum_{i=1}^N I_{zi} \right\} + \frac{1}{2} (\beta\hbar\omega_0)^2 \sum_{i=1}^N \sum_{j=1}^N I_{zi}I_{zj} + \dots \right) \quad (4)$$

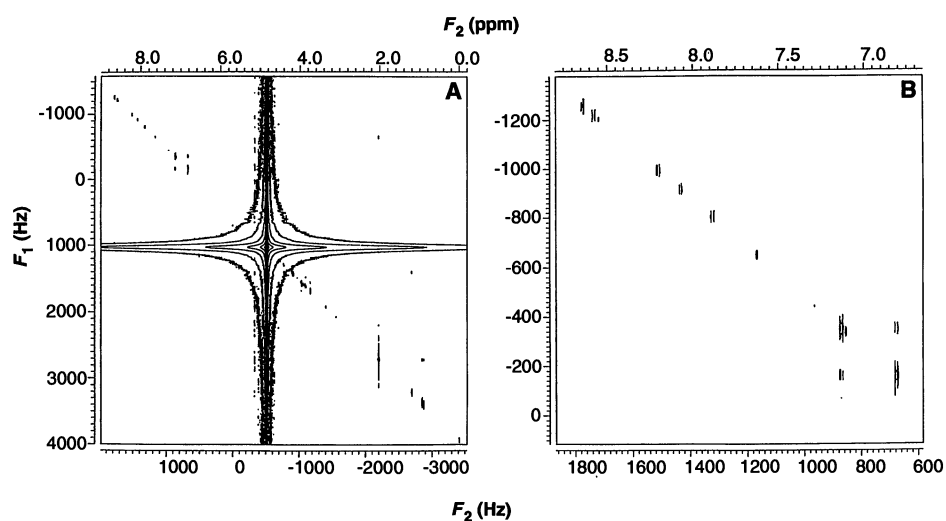


**Fig. 2.** (A) CRAZED spectrum of a 20 mM solution of the fibronectin fragment in water. The first gradient pulse was 1 ms long, with amplitude 6 G  $\text{cm}^{-1}$ . Joint solute-solvent two-quantum coherences are seen from most of the glycopeptide peaks. (B) Expanded view of a small portion of the spectrum showing the amide protons. Note that the Tyr aromatic doublets at  $F_2 = 6.85$  and 7.15 ppm (coupled in the normal COSY) produce both two-quantum water-peptide coherences ( $F_1 = -F_2 + 0.88$  ppm) and doublets of cross-peaks between each other.

The term in curved brackets in Eq. 4 is the starting point for essentially all work in high-resolution NMR. In fact, however, it has long been recognized that truncation to the bracketed term in Eq. 4 is not trivial to justify (15). The spin operator  $I_z = \sum I_{zi}$  has eigenvalues ranging from  $N/2$  to  $-N/2$ , which differ in energy by  $N\hbar\omega_0$ . For 1 ml of water,  $N = 7 \times 10^{22}$ , so  $N\hbar\omega_0 \gg kT$ . Of course, most of the eigenstates have nearly equal numbers of spins up and down; the actual (binomial) distribution of eigenstates is approximately Gaussian with  $\sigma = \sqrt{N}$ . However,  $\sigma\hbar\omega_0 \gg \beta^{-1}$  as well. A more careful analysis shows that truncation is valid as long as the correlations between states separated by energies at least comparable to  $\beta^{-1}$  are unimportant. Such states involve  $10^4$  or more spins, and thus ignoring them sounds quite reasonable—until one recognizes that each spin is coupled to  $N$  other spins in Eq. 1. In addition, each of the  $N^2$  ( $\sim 10^{45}$ ) terms  $I_{zi}I_{zj}$  in Eq. 4 is comparable in size to  $I_{zi}$ .

We now show that the combination of the long-range dipolar couplings in Eq. 1 and the additional terms in Eq. 4 can contribute significant signals (although nei-

ther term contributes much by itself). The density matrix derivation is straightforward starting from Eq. 1 and 4, so it will merely be outlined here (and illustrated schematically in Fig. 3). After the first  $(\pi/2)_y$  pulse, the density matrix is:

$$\rho = 2^{-N} \left( \left\{ 1 - \beta\hbar\omega_0 \sum_{i=1}^N I_{zi} \right\} + \frac{1}{2} (\beta\hbar\omega_0)^2 \sum_{i=1}^N \sum_{j=1}^N I_{zi}I_{zj} + \dots \right) \quad (5)$$

The (normally neglected) third term of Eq. 5 contains two-quantum and zero-quantum operators that evolve during the delay  $t_1$  (producing terms such as  $I_{yi}I_{xj}$ ). The next  $\pi/2$  pulse transforms such terms into two-spin, one-quantum operators such as  $I_{yi}I_{zj}$ . The two gradient pulses in the CRAZED sequence in Fig. 1 act as a two-quantum filter; observable signals come only from two-quantum operators in  $t_1$  that are translated into one-quantum operators by the second pulse. Finally, the Hamiltonian has bilinear operators such as  $D_{ij}I_{zi}I_{zj}$ ; because  $[I_{yi}I_{zj}, I_{zi}I_{zj}] \propto I_{xi}$ , these dipolar couplings can convert two-spin, one-quantum operators

into an observable signal during  $t_2$ .

Calculating the exact evolution under a normal dipolar Hamiltonian can be quite difficult. Fortunately, the calculation is simplified dramatically in our case because all of the retained dipolar couplings are extremely small. The sum of the absolute values of all of the couplings from a single spin (say spin 1) to all others

$$\sum_{j=1}^N |D_{1j}t|$$

can be enormous, as noted earlier, but

$$\sum_{j=1}^N |D_{1j}t|^2$$

is far smaller. Thus the largest contribution by far to the observable signal will come from terms that only use a single dipolar coupling to get to the observables  $I_{xi}$  or  $I_{yi}$  (as illustrated in Fig. 3). Since at least one dipolar coupling will be needed during  $t_2$  to produce the observable signal, this means we can ignore the dipolar couplings during  $t_1$ . The result is:

$$\begin{aligned} \rho(t_2) = & 3 \cdot 2^{-N-4} (\beta\hbar\omega_0)^2 t_2 \exp(-i\Delta\omega t_2 I_z) \\ & \times \sum_{i=1}^N \sum_{j=1}^N D_{ij} [(I_{xi} + I_{xj}) \sin(2\Delta\omega t_1) \\ & \quad \cos(\gamma G(s_i - s_j)T) \\ & \quad - (I_{yi} + I_{yj}) \cos(2\Delta\omega t_1) \cos(\gamma G(s_i - s_j)T)] \\ & \times \exp(i\Delta\omega t_2 I_z) \quad (+ \text{unobservable terms}) \quad (6) \end{aligned}$$

The magnitude of this CRAZED signal, written as a fraction of the signal produced by the full sample magnetization after a single  $\pi/2$  pulse [ $\rho = 2^{-N} (\beta\hbar\omega_0) I_x$ ] is:

$$S = \frac{3\beta\hbar\omega_0}{8} t_2 \sum_{j=1}^N |D_{1j} \cos(\gamma G s_j T)| \quad (7)$$

where we have replaced the double sum with  $N$  times the sum over the second spin, fixing  $i = 1$  and  $z_1 = 0$  for convenience. Equation 7 still appears to be a small signal because it has the term  $\beta\hbar\omega_0 \approx 10^{-4}$ . Appearances are deceiving. The sum in Eq. 7 can be replaced by an integral over the sample volume  $v$ :

$$\begin{aligned} S = & \frac{3}{32\pi} M_0 t_2 \gamma \mu_0 \times \int_v r^{-3} (3\cos^2\theta - 1) \\ & \cos(\gamma G s T) (r^2 \sin\theta) dr d\theta d\phi \quad (8) \end{aligned}$$

Equation 8 eliminates the extra factor of  $\beta\hbar\omega_0$  by introducing  $M_0$ , the equilibrium magnetization per unit volume. The quantity  $(\gamma\mu_0 M_0)^{-1}$  is the "dipolar demagnetizing time"  $\tau_d$  as noted above. The integral must be calculated over the entire sample volume, minus a sphere with radius  $r_{\text{cutoff}}$  from the origin. In the absence of the cos

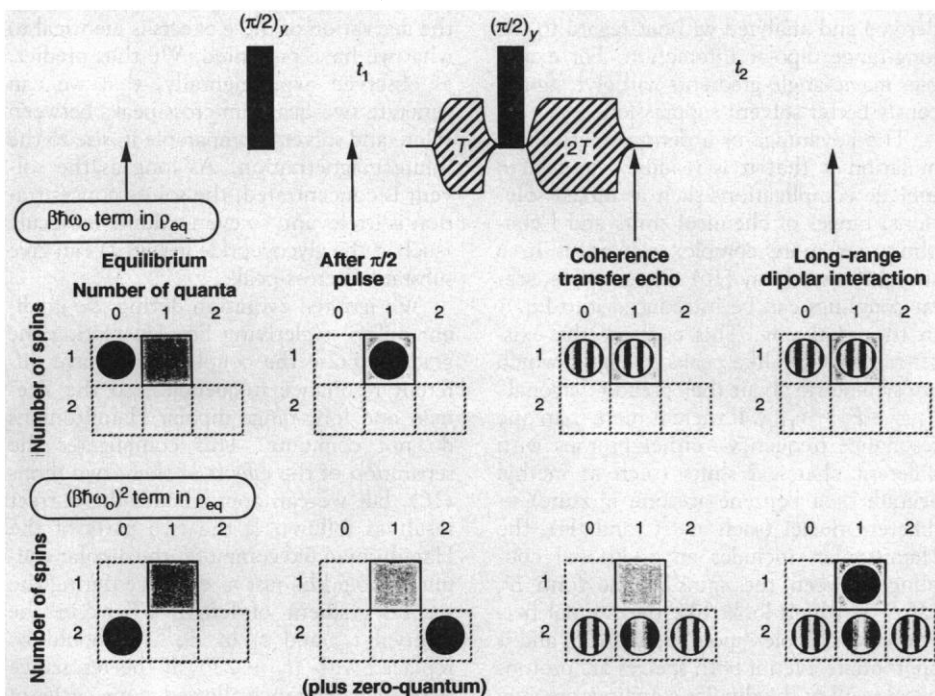


**Fig. 3.** Schematic illustration of the dominant pathway for generating observable signals from a CRAZED sequence. Black dots illustrate operators that are not spatially modulated. The black square represents the one-spin, one-quantum operators  $I_{xi}$  and  $I_{yi}$ , which are observable. The  $\beta\hbar\omega_0 I_z$  term in the equilibrium density matrix is a sum of one-spin, zero-quantum operators, which are turned into an observable signal during  $t_2$  by the first pulse. However, the coherence transfer echo imposes a strong spatial modulation on these operators, and they do not generate an observable signal during  $t_2$ . The  $(\beta\hbar\omega_0 I_z)^2$  term, on the other hand, gives a two-quantum operator during  $t_1$  (plus a zero-quantum operator that is omitted for clarity). The fraction of this two-quantum, two-spin operator which is transferred to one-quantum, two-spin operators by the coherence transfer echo is only mildly modulated. The dipolar couplings can then act to create an unmodulated, one-spin one-quantum operator (observable magnetization). The quantitative calculation in the text shows that very large signals are possible.

( $\gamma G s T$ ) term, it would vanish for a spherical sample. Figure 4 graphs the function  $F(\gamma G T r)$ , defined as:

$$\int_{\theta=0}^{\pi} \int_{\phi=0}^{2\pi} r^{-3} (3 \cos^2 \theta - 1) \cos(\gamma G s T) (r^2 \sin \theta) d\theta d\phi = (\gamma G T) F(\gamma G T r) \Delta \quad (9)$$

where  $\Delta = [3(\delta z)^2 - 1]/2$ ; the bulk of the signal comes from the range  $\gamma G T r \approx 2$  to 4. This result is easy to understand—when  $\gamma G T r \ll 1$ , the gradient is so small as to be unimportant, and the angular average makes the integral over  $\theta$  and  $\phi$  vanish; when  $\gamma G T r \gg 1$ , angular averaging is also effective.

The full integral in Eq. 9 can be solved numerically for any sample geometry, but is particularly simple at the center of a spherical sample of radius  $R$ . If  $\gamma G T R \gg 1$  (meaning the gradient pulse is strong enough to dephase the bulk magnetization) and  $\gamma G T r_{\text{cutoff}} T \ll 1$  (meaning the gradient pulse has little effect on a micrometer scale) we effectively just integrate Fig. 4 to get:

$$\int_{r=r_{\text{cutoff}}}^R \int_{\theta=0}^{\pi} \int_{\phi=0}^{2\pi} r^{-3} (3 \cos^2 \theta - 1) \cos(\gamma G s T) \times (r^2 \sin \theta) dr d\theta d\phi \approx -8.4 \Delta \quad (10)$$

This limit is easy to achieve in practice. Combining Eqs. 8 and 10 gives:

$$\text{CRAZED signal} = 0.25 t_2 \Delta / \tau_d \quad (11)$$

Equation 11 is a remarkable result. For  $t_2 \approx \tau_d$  the signal is comparable to the normal magnetization of the sample for a concentrated species (such as the solvent peak). The extra factor of  $\beta \hbar \omega_0 \approx 10^{-4}$  has disappeared into the dipolar demagnetizing time  $\tau_d$ . The observable signal is proportional to  $t_2$  for small values of  $t_2$ , but independent of  $t_1$  and  $G$  (if the gradient pulses are short and  $\gamma G T R \gg 1$ ). The  $G$  independence can be understood from Fig. 4, which shows that the major contribution to the integral comes from distances between roughly  $2/\gamma G T$  and  $4/\gamma G T$ . If  $G$  were doubled, the average dipolar coupling to this region would grow by a factor of 8 ( $1/r^3$ ); but the volume of the region would fall by a factor of 8.

Predictions of the  $t_1$  and  $t_2$  dependence are borne out experimentally for  $z$ -gradients ( $\Delta = 1$ ). The derivation above includes some approximations. The most important limitation is the perturbative expansion in  $t_2$ ; terms that come in to higher powers of  $t_2$  will of course eventually destroy the magnetization. However, experiments (Fig. 5) show that the range of validity of this expansion is comparable to  $\tau_d$ , which is

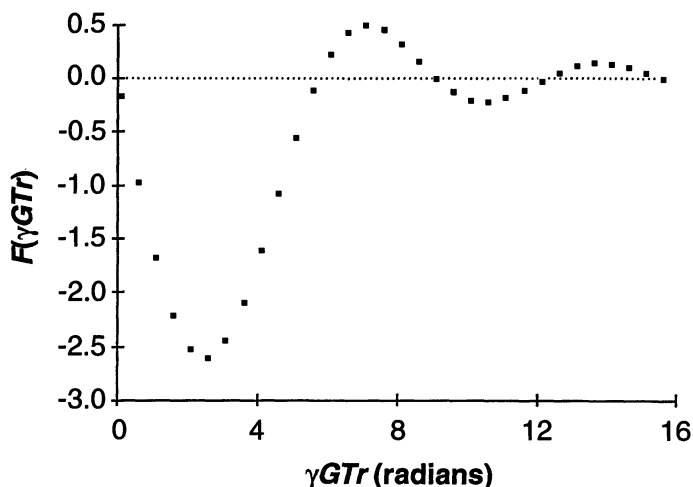


Fig. 4. The function  $F(\gamma G T r)$ , which gives the value of the integral in Eq. 9. Physically,  $F(\gamma G T r)$  is the effectiveness of the long-range part of the dipolar Hamiltonian in transferring coherence from slowly modulated two-spin operators such as  $I_{xi} I_{zj} \cos [\gamma G (s_i - s_j) T]$  in the shell at radius  $r$  into observable magnetization.

$\sim 80$  ms for this sample (80%  $\text{H}_2\text{O}$ ).

Note that magic-angle gradients ( $\Delta = 0$ ) are predicted to eliminate these effects completely, at least for this simple sequence. We have also verified this experimentally. Such pulses will remove a variety of “artifacts” from 2D spectra that were derived and analyzed without regard to the long-range dipolar interaction. For example, magic-angle gradients will give significantly better solvent suppression.

The advantage of a density matrix formulation is that it is readily extended to include complications such as mixed solutions, ranges of chemical shifts and  $J$  couplings, or more complex sequences in a straightforward way (16). For example, scalar couplings can be introduced into Eq. 1 in the usual way. This explains the existence of COSY-like peaks in Fig. 2 which are symmetric about the “pseudo-diagonal”  $F_1 = -F_2 - \nu_{\text{H}_2\text{O}}$ . If there is more than one resonance frequency—either protons with different chemical shifts (such as methyl acetate or a benzene-acetone mixture) or different nuclei (such as  $^{13}\text{C}$  and  $^1\text{H}$ ), the Hamiltonian includes an additional coupling between the spins of the form  $D_{ij} (2I_{zi} S_{zj})$ , which looks like the normal heteronuclear dipole-dipole interaction, and is appropriate even if both species are protons because all of the dipolar couplings are very small. This is equivalent to the “first-order spectrum” approximation made to truncate the scalar coupling if it is small compared to the chemical shift differences.

The equilibrium density matrix now has  $\mathbf{N} \cdot \mathbf{M}$  terms of the form  $I_{zi} S_{zj}$ , which are rotated into  $I_{xi} S_{xi}$  by a single  $\pi/2$  pulse. These terms evolve at the sum (two-quantum coherences) and difference (zero-quantum coherences) of the chemical shifts. The two-quantum term survives the coherence

transfer echo (exactly as before) when the second  $\pi/2$  pulse creates operators such as  $I_{zj} S_{yi}$ . Finally, the dipolar couplings act during  $t_2$  to transform these operators into  $S_{xi}$  or  $I_{xi}$ . Except for a small difference in the numerical coefficient (which scales down production of  $I_{xi}$  and  $I_{yi}$  by a factor of 2/3), the derivation of these effects is identical to what we have presented. We thus predict, as observed experimentally, that we can generate two-quantum cross-peaks between solute and solvent comparable in size to the solute magnetization. As long as the solvent is concentrated, the solute concentration is irrelevant; so even a dilute molecule (such as the glycopeptide in Fig. 2) can give substantial cross-peaks.

We ignored evolution during the gradient pulses in deriving Eq. 11. During the gradient pulse the coupled spins have different resonance frequencies, so the Zeeman and long-range dipolar Hamiltonians do not commute. This complicates the separation of the effects of these two terms (16), but we can approximate the correct result as follows. If the two parts of the Hamiltonian did commute, the dipolar couplings would be just as effective during the second gradient of length  $2T$  as in the interval  $t_2$ , and  $t_2$  in Eq. 11 should be replaced with  $(t_2 + 2T)$ . If the resonance frequency difference allowed many cycles of evolution, we should replace the full dipolar Hamiltonian  $3I_{zi} I_{zj} - \mathbf{I}_i \cdot \mathbf{I}_j$  with the truncated version  $2I_{zi} I_{zj}$  during that pulse, and this scales down the rate of CRAZED signal generation by a factor of 2/3 during the  $2T$  gradient pulse. Thus

$$0.25(t_2 + 1.33T)\Delta/\tau_d \leq \text{CRAZED signal} \leq 0.25(t_2 + 2T)\Delta/\tau_d \quad (12)$$

Experimentally, the intercept is approxi-

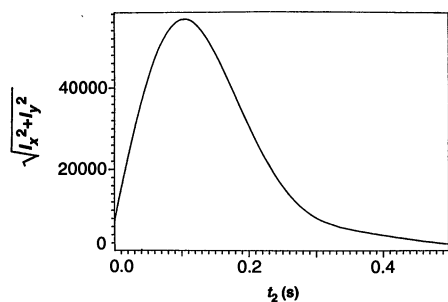


**Fig. 5.** Time-domain slice  $S(t_1 = 2.5 \text{ ms}, t_2)$  of the CRAZED spectrum in Fig. 2. Note the rapid growth of the signal after the gradient pulses end. The experimental data confirm the predictions of Eqs. 11 and 12.

mately  $t_2 \approx -1.8 \text{ T}$ , in agreement with Eq. 12. Experimentally the slope is also nearly independent of  $t_1$  and the length of the gradient pulses. The signal for  $t_1 = t_2 = 0$  in a Bloch equation treatment (4) is  $0.5 \text{ T}\Delta/\tau_c$ , which agrees perfectly with the upper limit in Eq. 12 above but is somewhat larger than we observe. Long gradient pulses modulate the magnetization on a distance scale comparable to diffusion lengths, and the signal decreases dramatically (17).

We have seen zero-, three-, or four-quantum coherences as well by altering the ratio of the gradient pulse lengths. A 1:3 ratio of gradient pulses in Fig. 1 (three-quantum selection) gives the dominant peak at ( $F_1 = -3\nu_{\text{H}_2\text{O}}, F_2 = \nu_{\text{H}_2\text{O}}$ ), and a "pseudo-diagonal" of glycopeptide resonances, all with  $F_1 = -F_2 - 2\nu_{\text{H}_2\text{O}}$ . These are all three-quantum resonances, involving two water protons and one glycopeptide peak. These effects arise in a density matrix treatment from terms proportional to higher powers of  $\beta\hbar\omega_0$  in  $\rho_{\text{eq}}$ . Three-quantum operators are produced when the next term

$$\left[ \frac{1}{6} (\beta\hbar\omega_0)^3 \sum_{i=1}^N \sum_{j=1}^N \sum_{k=1}^N I_{zi} I_{zj} I_{zk} \right]$$

is rotated by the first pulse. A three-quantum gradient filter in a CRAZED experiment would save these coherences, which are transformed into observable magnetization during  $t_2$  by the second commutator with the dipolar Hamiltonian. Thus the signal will be proportional to  $t_2^2$ . The next term [proportional to  $(\beta\hbar\omega_0)^4$ ] gives four-quantum coherences. Thus, for all practical purposes, the power series expansion in Eq. 4 does not converge. Ordinarily (in dilute samples), the extra terms which are ignored by the conventional high-temperature approximation never become observable signals, so the approximation leads to reasonable results. If one species is concentrated, and gradient echoes are used, the dynamics is far richer and more complex—an important subtlety which has been ignored until now.

Our treatment explains many common observations about NMR of proteins in water. For example, it is well known in the biological NMR community that putting the water peak off resonance "overloads the spectrometer" and produces "distortions." In fact, all that does is separate these additional resonances from the expected peaks. Even when the water is on resonance, these multiple-quantum peaks change peak intensities and degrade the apparent performance of a coherence transfer echo. It is also common practice to use massive gradient pulses (for example, 1 ms at  $30 \text{ G cm}^{-1}$ ) for good water suppression or heteronuclear  $^1\text{H}$ - $^{13}\text{C}$  coherence transfer echoes. Such a pulse dephases a 1-cm sample by more than 700 radians across its length, and would seem excessive. In fact, weaker pulses do not work as well. With such gradient pulses, the pitch of the magnetization helix becomes smaller than the diffusion length, so the intermolecular multiple-quantum peaks fail to refocus. In the heteronuclear  $^1\text{H}$ - $^{13}\text{C}$  case, an additional effect contributes—the 1:3.978 ratio of pulse lengths needed is perilously close to the 1:4 ratio that saves the four-quantum peak of water, and thus the water peak must be made extremely "sharp" with a strong gradient for solvent suppression to work.

If magic-angle gradients are used, far weaker gradient pulses will perform well, with significant simplifications in hardware and reduction in settling artifacts. Thus, we believe that the nearly universal practice of using  $z$ -axis gradient pulses in concentrated solvents should be terminated, unless the experimenter is actually interested in producing these additional resonances (or can totally dephase the solvent magnetization in other ways). For existing pulse sequences, derived without taking the dipolar interaction into account, this precaution should restore confidence in the interpretation of intensities from cross-peaks.

Much remains to be investigated, both theoretically and experimentally, but enhancing these extra resonances may well be useful in certain applications. Because the dipolar interaction between spins at the same frequency ( $3I_{zi}I_{zj} - \mathbf{I}_i \cdot \mathbf{I}_j$ ) has different symmetry properties than does the truncated version  $2I_{zi}I_{zj}$ , appropriate for spins at different frequencies, it should be possible to detect water-biomolecule two-quantum coherences without interference from water-water two-quantum coherences (for example, by a dipolar line narrowing sequence or by magic-angle spinning with gradient pulses). It may also be true that nonlinear gradients will be useful in amplifying these coherences.

Finally, we note a potentially important application of these effects in magnetic resonance imaging. Multiple echoes have previously been observed in imaging experiments, but the spatial localization of these signals

cannot be appreciated from a Bloch-equation treatment (which essentially assumes an infinitely large sample). Our density matrix treatment shows that the signal comes directly from pairs of spins separated by approximately one-half turn of the magnetization helix (see Fig. 4). This distance can be adjusted to any value from  $\approx 1 \mu\text{m}$  on up by varying the gradient strength and length. Thus, for example, the intensity of a two-quantum peak between water and a dilute molecule inside a cell or vesicle would directly measure the radial distribution function of the water concentration, and this might correlate with local structural abnormalities.

## REFERENCES AND NOTES

- See, for example, R. R. Ernst, G. Bodenhausen, A. Wokaun, *Principles of Nuclear Magnetic Resonance in One and Two Dimensions* (Clarendon, Oxford, 1987).
- M. McCoy and W. S. Warren, *J. Chem. Phys.* **93**, 858 (1990).
- W. S. Warren, Q. He, M. McCoy, F. C. Spano, *ibid.* **96**, 1659 (1992).
- Q. He *et al.*, *ibid.* **98**, 6779 (1993).
- A. Abragam, *The Principles of Nuclear Magnetism* (Clarendon, Oxford, 1961).
- A. Bax *et al.*, *Chem. Phys. Lett.* **69**, 567 (1980); A. A. Maudsley, A. Wokaun, R. R. Ernst, *ibid.* **55**, 9 (1978).
- A. Pines, "Lectures on Pulsed NMR," presented at the 100th Fermi School on Physics, Varenna, Italy, 1986; D. P. Weitekamp, *Adv. Magn. Reson.* **11**, 111 (1983).
- H. Matsuura *et al.*, *J. Biol. Chem.* **263**, 3314 (1988).
- G. Deville, M. Bernier, J. M. Delrieux, *Phys. Rev. B* **19**, 5666 (1979).
- D. Einzel, G. Eska, Y. Hirayoshi, T. Kopp, P. Wölflé, *Phys. Rev. Lett.* **53**, 2312 (1984).
- R. Bowtell, R. M. Bowley, P. Glover, *J. Magn. Reson.* **88**, 643 (1990).
- H. Körber *et al.*, *ibid.* **93**, 589 (1991).
- A. S. Bedford *et al.*, *ibid.* **93**, 516 (1991).
- R. Bowtell, *ibid.* **100**, 1 (1992).
- See, for example, A. Abragam and M. Goldman, *Nuclear Magnetism: Order and Disorder* (Clarendon, Oxford, 1982), chap. 5; C. P. Slichter, *Principles of Magnetic Resonance* (Springer-Verlag, Berlin, 1990), appendix E.
- W. Richter, S. Vathyam, W. S. Warren, unpublished results.
- For example, with the  $0.06 \text{ T m}^{-1}$  gradient used for the experiments in this report, the linewidth of a 1-cm sample is  $160 \text{ krad s}^{-1}$  (25 kHz). With a 10-ms gradient, the magnetization undergoes a 1 radian phase shift with translation of only  $6 \mu\text{m}$ . The root-mean-square displacement of water in 10 ms due to self-diffusion ( $\sigma = \sqrt{2Dt}$ ) is  $\sim 7 \mu\text{m}$ . As this would predict, we find experimentally that the signal weakens for gradient lengths more than a few milliseconds. In our previously published experiments (4) we used gradients that were about a factor of 10 weaker, and then gradient pulse lengths of 15 to 30 ms gave substantial signals.
- W.S.W. is pleased to acknowledge helpful and stimulating conversations with J. Jeener, P. Broekart, and A. Vlassenbroek during a recent visit to Brussels and with L. Müller at Bristol-Myers-Squibb. We would also like to thank D. Mattiello, M. Cummings, and P. Hornung at Varian Associates for their instrumental assistance in performing the CRAZED experiments using magic-angle gradients. Supported in part by the National Institutes of Health under grant GM35253 (W.S.W.).

1 July 1993; accepted 9 November 1993